AIMS Energy, 9(5): 1043–1066.
DOI: 10.3934/energy.2021048
Received: 04 June 2021
Accepted: 23 August 2021
Published: 29 September 2021

http://www.aimspress.com/journal/energy

Research article

A design and performance prediction method for small horizontal axis wind turbines and its application

Stephen K. Musau[1,*], Kathrin Stahl[2], Kevin Volkmer[2], Nicholas Kaufmann[3] and Thomas H. Carolus[2]

[1] Department of Mechanical Engineering, Dedan Kimathi University of Technology, Private Bag—10143, Nyeri, Kenya
[2] Institute for Fluid-and Thermodynamics, University of Siegen, 57068 Siegen, Germany
[3] SCHOTTEL HYDRO GmbH, Mainzer Strabe 99 56322, Germany

* **Correspondence:** Email: Stephen.musau@dkut.ac.ke; Tel: +254726859185.

Abstract: The paper deals with small wind turbines for grid-independent or small smart grid wind turbine systems. Not all small turbine manufacturers worldwide have access to the engineering capacity for designing an efficient turbine. The objective of this work is to provide an easy-to-handle integrated design and performance prediction method for wind turbines and to show exemplary applications.

The underlying model for the design and performance prediction method is based on an advanced version of the well-established blade-element-momentum theory, encoded in MATLAB™. Results are (i) the full geometry of the aerodynamically profiled and twisted blades which are designed to yield maximum power output at a given wind speed and (ii) the non-dimensional performance characteristics of the turbine in terms of power, torque and thrust coefficient as a function of tip speed ratio. The non-dimensional performance characteristics are the basis for the dimensional characteristics and the synthesis of the rotor to the electric generator with its load.

Two parametric studies illustrate typical outcomes of the design and performance prediction method: A variation of the design tip speed ratio and a variation of the number of blades. The predicted impact of those parameters on the non-dimensional performance characteristics agrees well with common knowledge and experience.

Eventually, an interplay of various designed turbine rotors and the given drive train/battery charger is simulated. Criterions for selection of the rotor are the annual energy output, the rotor speed at design wind speed as well as high winds, and the axial thrust exerted on the rotor by the wind. The complete rotor/drive train//battery charger assembly is tested successfully in the University of Siegen wind tunnel.

Keywords: small horizontal axis wind turbine; design; performance prediction; blade element momentum

1. Introduction

Three trends in generating and providing electricity can be observed: Firstly, utilizing free primary, i.e., renewable energy, avoiding the cost for CO_2-emission certificates and other end-of-lifetime waste disposal cost. Secondly, distributed small and volatile energy resources are combined into a small smart grid to improve reliability and robustness of decentralized grids. "Smart" in this context implies the control of the production and distribution utilizing smart meters, smart appliances, storage facilities like batteries and renewable energy resources. This can be of particular interest for rural electricity distribution networks and the future infrastructure required for electric vehicles. As an example, within its Seventh framework programme, the European Commission supported numerous projects like "Open Systems for Energy Services", "Smart … rural grid innovating resilient electricity distribution infrastructures, services and business models", "Scalable energy management infrastructure for aggregation of households" (FP7 [1]). Thirdly, in some cases the cost for feeding the power into a grid (or reversely drawing electricity from a grid) may exceed all other cost. A link-up to a public grid even may be economically impossible in remote areas.

This paper exclusively deals with small horizontal axis wind turbines (HAWT) for grid-independent or small smart grid systems, Figure 1. Obviously, the current and future demand provides enough support to sustain a significant number of manufacturers. In highly industrialized areas of the world, advanced methods allow manufacturing at high levels of quality and even mass production, whereas in other parts of the world simple manufacturing techniques are necessary, Figure 2. In the past ill-conceived small wind turbines have damaged the reputation for such machines. Today standards and testing institutions increasingly provide consumers with realistic and comparable performance ratings of competing products. Examples are the British small wind turbine standard [2], the German annual market survey on small wind turbines [3] and the Austrian small turbine test field Energie-For Schungspark Lichtenegg [4]. On the other hand, not all small turbine manufacturers, especially the small batch producers, may have access to the engineering capacity to design an efficient turbine.

A number of studies have been undertaken on wind turbines focusing on structural analysis, rotor dynamics and optimization of the shape of wind turbines. Yuan chang Chen *et al.* [19,20] and Wel Chen *et al*. [21], recently studied and reported extensively on the dynamics of the blade rotor and blade modeling. Many computational approaches have also found applications in aerodynamic design of wind turbines such as computational Fluid Dynamics (CFD), Wake Method and Blade Momentum (BEM) theory. BEM theory is widely used in aerodynamic design of wind turbines due to its simplicity and accuracy [26]. With blade optimization, power coefficient close to Betz limit of 59.2% can be realized with wind turbines.

On aerodynamics performance optimization, a number of studies are reported in the literature [22–24]. Ceyhan [22] undertook a study on the aerodynamic performance optimization of horizontal axis wind turbine blades using the BEM theory and genetic Algorithm. In the study, the chord and twist distribution were the key variables during the design and were optimized for optimum power production. Using differential evolution method, Clifton- Smith and wood [23], undertook a

research with the aim of maximizing power coefficient and minimizing the starting time of small wind turbines blades. Liu *et al*. [24], developed an optimization method for wind turbines blades in order to maximize the annual energy output. A 7.5% increase in the annual energy output was realized in the study. Meng-Hsien [25], undertook a different study both numerically and experimentally on a small wind turbine blade, where one blade was designed using the BEM theory and the other was non-twisted blade. It was found out that the blade designed with BEM theory had higher coefficient of performance compared to the non-twisted blade.

Most wind turbines optimizations are conducted for wind turbines working in on design conditions. Wind turbines are exposed to different working conditions. In addition, matching the electric generator to the turbine performance characteristics curves is fundamental in ensuring the components are protected against extreme design effects.

Figure 1. Examples of micro and small wind turbines in the Netherlands.

Figure 2. Examples of small batch turbine manufacturing; left: rural workshop in Kenya, middle: wooden blade carved with the help of a grid of drill holes of precise depth (requiring a standard carpenter's workshop only); right: CNC-milled mold for a carbon fiber composite manual blade manufacture in Germany.

Hence, the objective of the paper is to report a procedure for designing blades for small HAWTs. The turbine rotor with these blades should yield a shaft power as close as possible to theoretical maximum and match best to a given electric generator. The underlying theory is an advanced version

of the well-established blade-element-momentum (BEM) theory, encoded in our own in-house MATLAB™ code *deapWind*[1] and validated extensively Kaufmann [5]. Eventually, as an exemplary case study, this paper describes the design of a small generator/battery charger with a 1 m diameter turbine rotor. Starting point is a one-year histogram of measured wind speed at the candidate site at Dedan Kimathi University of Technology in rural central Kenya. Upon design and manufacturing, a concluding wind tunnel experiment demonstrates how well the methodology works.

2. Design and performance calculation procedure

The turbine design methodology comprises three fundamental steps: (i) The design of the HAWT rotor, especially its profiled and twisted blades, (ii) the prediction of its performance characteristics in terms of shaft power, shaft torque and axial thrust force on the complete rotor, (iii) the overall power produced when "loaded" by the torque from the electric generator. Upon this last steps, it is straightforward to determine the overall electric power output for a given—say annual—wind speed histogram. Eventually, measures to achieve low cut-in wind speed and switch-off features for high winds have to be designed. The latter steps are out of the scope of this paper.

2.1. Aerodynamic design of rotor blades

The blade design is based on the standard GLAUERT/SCHMITZ blade element momentum (BEM) theory as described for instance Gasch and Twele [6] or Gerhard *et al.* [7]). It is summarized only briefly; some more details are presented in the following section. The turbine design process starts with the specification of:

- the design wind speed far upstream of the turbine $c_{0,design}$,
- the design rotor diameter D_{tip} (= $2r_{tip}$),
- the density of the air ρ, the turbine will operate with, and
- the design tip speed ratio λ_{design}, of the turbine

$$\lambda_{design} \equiv \frac{u_{tip}}{c_{0,design}} = \frac{\pi D_{tip} n}{c_{0,design}} \tag{1}$$

with the circumferential velocity of the blade tip due to its rotation u_{tip} and the rotor speed n.

Essentially, $c_{0,design}$ and D_{tip} determine the power harvested by the turbine, and λ_{design}, its rotational speed for a given $c_{0,design}$. Each blade is thought as a number of blade elements (BE) with a small radial size δr, stacked from root to tip, Figure 3 left. The BEs in a coaxial strip form themselves into an elementary blade cascade (CA). The most relevant geometrical parameters of each local BE are, Figure 3 right,

- the chord length, l,
- the pitch angle, γ,
- the angular distance, t, between two circumferentially adjacent BE's,
- the number of blades, B, and
- the solidity, σ, of the CA

$$\sigma \equiv \frac{\ell}{t} = \frac{\ell}{2\pi r/B} \tag{2}$$

Figure 4 left shows schematically a wind turbine with a boundary stream tube. The free stream wind speed far upstream, c_0 is decelerated to c_3 far down stream in the wake. c_3 comprises a circumferential velocity component c_{u3} (i.e., the swirl) and an axial (= meridional) c_{m3}. The spatially averaged velocities at the entrance and exit plane of a CA are depicted in Figure 4 right. c's indicates absolute frame of reference, w's rotating frame of reference flow velocities; u is the circumferential velocity of the CA due to the rotation of the rotor. Again, c_2 comprises a circumferential and a meridional velocity component c_{u2} and c_{m2}, respectively. Instead of carrying on with dimensional quantities, the standard GLAUERT/SCHMITZ theory deals with the non-dimensional axial and tangential induction factors

$$a \equiv 1 - \frac{c_m}{c_0} \text{ with } c_m = c_1 = c_{m2} \text{ and } \quad a' \equiv -\frac{1}{2}\frac{c_{u2}}{u} . \tag{3a, b}$$

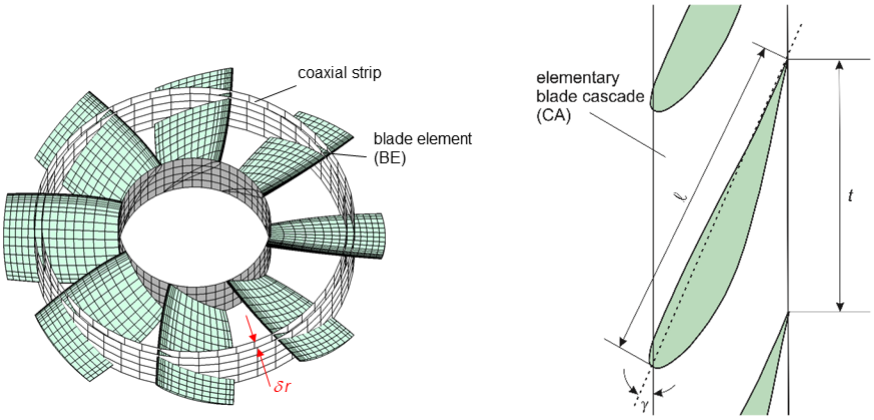

Figure 3. Left: Segmentation of a turbine rotor into coaxial strips; right: Elementary blade cascade (CA).

For maximum power extraction from the wind the classic BETZ theory [8] requires

$$c_m = \frac{1}{2}(c_0 + c_{m3}) \tag{4}$$

which is assumed to hold true, also within the GLAUERT/SCHMITZ theory. The outcome of the combined application of the axial and angular momentum conservation are design values of a and a' or in other words, the kinematics of the flow, each local BE ensures in order to provide maximum power output at a specified design wind speed, $c_{0,\,design}$. The design values of a and a' are depicted in Figure 5. They are functions of the relative radial position r/r_{tip} and λ_{design} of each BE considered.

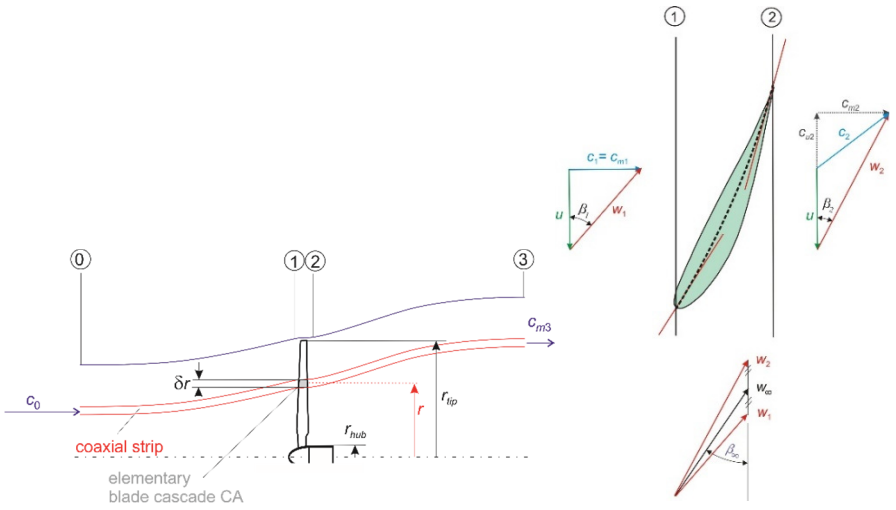

Figure 4. Left: Wind turbine rotor in boundary stream tube; right: Velocity triangles at the rotor entrance and exit planes; the dashed black line indicates the blade profile mean line.

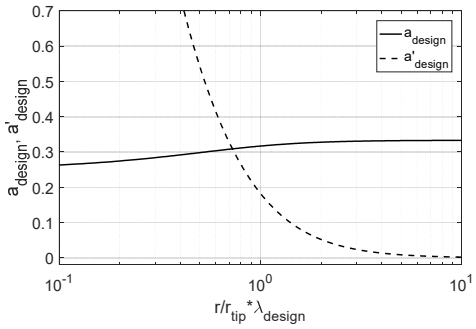

Figure 5. Design induction factors for maximum power (GLAUERT/SCHMITZ theory).

The effect of any flow deflecting elementary blade cascade CA is attributed to lift and drag forces δL and δD from all BE's in the CA which are considered to be isolated infinite span airfoil sections aligned to the free stream incoming flow velocity w_∞ with an angle of attack α, Figure 6 left. Key parameters of an airfoil sections are its lift coefficient C_L and its drag/lift ratio ε, defined as

$$C_L \equiv \frac{\delta L}{\frac{1}{2}\rho w_\infty^2 \ell \delta r}, \quad \varepsilon \equiv \frac{C_D}{C_L} \text{ with } \quad C_D \equiv \frac{\delta D}{\frac{1}{2}\rho w_\infty^2 \ell \delta r}. \tag{5a, b, c}$$

The airfoil shape is chosen by the designer, who also has to identify the $C_L(\alpha)$ and $C_D(\alpha)$ from wind tunnel data or other sources. The inflow velocity to each BE corresponds to the vector mean of the inlet and outlet relative velocities w_1 and w_2; its magnitude is

$$w_\infty = \frac{1}{2}\sqrt{4c_{m,1}^2 + (2u - c_{u2})^2} = c_0\sqrt{(1 - a_{design})^2 + (1 + a'_{design})^2\left(\frac{r}{r_{tip}}\lambda_{design}\right)^2} \tag{6}$$

and the flow angle

$$\beta_\infty = \arctan\left(\frac{2c_{m,1}}{2u - c_{u2}}\right) = \arctan\left(\frac{1 - a_{design}}{1 + a'_{design}} \frac{r_{tip}}{r} \frac{1}{\lambda_{design}}\right) \tag{7}$$

Eventually, this results in the solidity of each elementary blade cascade CA.

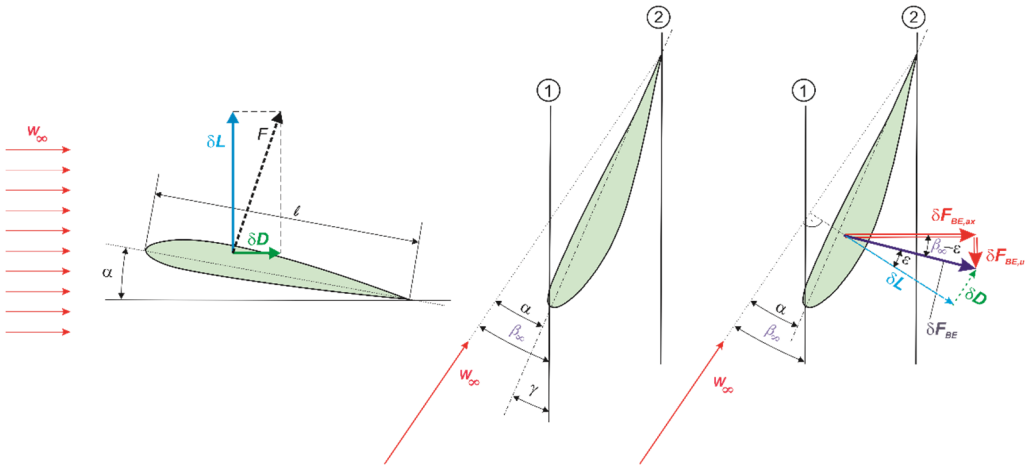

Figure 6. Left: Lift and drag force on an 2D airfoil section in a wind tunnel—aligned to mean flow direction with an angle of attack, α; middle: Transformation of the 2D airfoil section into a BE; right: Aerodynamic force components on a BE.

$$\sigma_{design}\left(\frac{r}{r_{tip}}\right) = \frac{4a'_{design} \frac{r}{r_{tip}} \lambda_D}{C_{L,D}\left(1 - a_{design}\right)\left(1 - \varepsilon_{design} \frac{r}{r_{tip}} \lambda_D \frac{1 + a'_{design}}{1 - a_{design}}\right)\sqrt{1 + \left(\frac{1 + a'_{design}}{1 - a_{design}}\right)^2 \left(\frac{r}{r_{tip}} \lambda_{design}\right)^2}}. \tag{8}$$

and the pitch angle

$$\gamma_{design} = \beta_\infty - \alpha_{design}. \tag{9}$$

In our implementation the public domain software XFOIL (Drela, [9,10]) is integrated, which yields the airfoil lift and drag coefficients as a function of the chosen airfoil shape, angle of attack and the Reynolds number

$$\mathrm{Re} = \frac{w_\infty \ell}{\nu}, \tag{10}$$

ν being the kinematic viscosity of the air.

Finally, the geometrical parameters σ_{design}, hence l for the chosen number B of rotor blades, and γ_{design} are sufficient to draw the blades and the complete rotor.

2.2. Prediction of aerodynamic rotor performance

The goal of this analysis is the aerodynamic performance of the rotor with its geometry as found in the previous section. Among others the shaft power, the shaft torque and the axial thrust the rotor

experiences due to the incoming wind are most relevant. These quantities are not only of interest at its design point λ_{design}, but also at all off-design operating points (i.e., at arbitrary values of $\lambda \equiv \pi D_{tip} n / c_0$) — preferably in terms of the non-dimensional power, torque and thrust coefficients

$$C_P \equiv \frac{P_S}{\frac{\rho}{2}\frac{\pi}{4} D_{tip}^2 c_0^3},\ C_M \equiv \frac{M_S}{\frac{\rho}{2}\frac{\pi}{8} D_{tip}^3 c_0^2} \left(= \frac{C_P}{\lambda}\right) \text{ and } C_T \equiv \frac{F_{ax}}{\frac{\rho}{2}\frac{\pi}{4} D_{tip}^2 c_0^2} \tag{11a, b, c}$$

$C_P(\lambda)$, $C_M(\lambda)$ and $C_T(\lambda)$ are the non-dimensional performance characteristics of the turbine.

The method chosen for estimating the performance characteristics is again based on the blade element momentum (BEM) theory, although refined for reasons of accuracy. In contrast to the design method, the flow velocities, or synonymously a and a', and the angle of attack, α, hence lift and drag at each BE need to be computed for arbitrary values of λ. For the sake of completeness, some more steps, which have been omitted in section 2.1 are presented in this section. Full details can be found in Kaufmann [5].

Starting point is the conservation of axial momentum applied to the fluid in a coaxial strip from 0 to 3 as in Figure 4 left. It yields the axial force acting on the elementary blade cascade CA

$$\delta F_{ax,CA} = (c_0 - c_{m3})\delta \dot{m} \ . \tag{12}$$

The mass flow rate through the CA is

$$\delta \dot{m} = \rho c_{m1} \delta A = \rho c_{m1} 2\pi r \delta r \ . \tag{13}$$

The theoretical shaft power is obtained via EULER's turbine equation (i.e., conservation of angular momentum, friction ignored) as

$$\delta P_{th,CA} = u\left(c_{u2} - c_{u1}\right)\delta \dot{m}$$

Eventually, with the definitions of the induction factors Eq (3a,b), the CA thrust and power coefficients become;

$$C_{T,CA} \equiv \frac{\delta F_{ax,CA}}{\rho c_0^2 \pi r \delta r} = 4a(1-a) \tag{14a}$$

and

$$C_{P,th,CA} \equiv \frac{\delta P_{th,CA}}{\rho c_0^3 \pi r \delta r} = 4a'(1-a)\left(\frac{r}{r_{tip}}\lambda\right)^2 , \tag{14b}$$

respectively. For any given value of λ, the two Eq (14a,b) bear the four unknown quantities $C_{T,CA}$, $C_{P,th,CA}$, a and a'. Additional equations are obtained by considering each CA as a set of isolated BE's experiencing a lift and a drag force. Referring to Figure 6 right the force components on one BE in the CA are

$$\delta F_{BE,ax} = \frac{1}{2}\rho w_\infty^2 \left(C_L \cos\beta_\infty + C_D \sin\beta_\infty\right) \ell \delta r \tag{15a}$$

and

$$\delta F_{BE,u} = \frac{1}{2}\rho w_\infty^2 \left(C_L \sin\beta_\infty - C_D \cos\beta_\infty\right) \ell \delta r \,. \tag{15b}$$

Eventually, the local thrust and power coefficient of the complete CA (consisting of B BE's) are obtained as

$$C_{T,CA}\left(\equiv \frac{B\delta F_{ax,BE}}{\rho c_0^2 \pi r \delta r}\right) = \frac{B\ell r_{tip}}{2\pi \dfrac{r}{r_{tip}}}\left((1-a)^2 + \left(\frac{r}{r_{tip}}\lambda\right)^2 (1+a')^2\right)\left(C_L \cos\beta_\infty + C_D \sin\beta_\infty\right) \tag{16a}$$

and

$$C_{P,CA}\left(\equiv \frac{B\delta P_{BE}}{\rho c_0^3 \pi r \delta r}\right) = \frac{B\ell r_{tip}}{2\pi \dfrac{r}{r_{tip}}}\left((1-a)^2 + \left(\frac{r}{r_{tip}}\lambda\right)^2 (1+a')^2\right)\left(C_L \cos\beta_\infty - C_D \sin\beta_\infty\right)\frac{r}{r_{tip}}\lambda \,, \tag{16b}$$

respectively. Eventually, equating $C_{T,CA}$ from Eq (14a) and (16a) and $C_{P,th,CA} = C_{P,CA}$ from Eq (14b) and (16b) yields two non-linear equations for the two unknowns a and a' for any λ considered:

$$4a(1-a) = \frac{B\ell r_{tip}}{2\pi \dfrac{r}{r_{tip}}}\left((1-a)^2 + \left(\frac{r}{r_{tip}}\lambda\right)^2 (1+a')^2\right)\left(C_L \cos\beta_\infty + C_D \sin\beta_\infty\right) \tag{17a}$$

$$4a'(1-a)\left(\frac{r}{r_{tip}}\lambda\right) = \frac{B\ell r_{tip}}{2\pi}\left((1-a)^2 + \left(\frac{r}{r_{tip}}\lambda\right)^2 (1+a')^2\right)\left(C_L \cos\beta_\infty - C_D \sin\beta_\infty\right)\lambda \tag{17b}$$

So far the analysis refers to one CA at r/r_{tip}. The overall turbine thrust and power coefficients, i.e., the targeted characteristics of the complete rotor, are obtained by summation over all CA's:

$$C_T(\lambda)\left(\equiv \frac{F_{ax}(\lambda)}{\frac{1}{2}\rho c_0^2 \frac{\pi D_{tip}^2}{4}}\right) = \frac{\sum\limits_{\text{all CA's}} C_{T,CA}(\lambda) 2\pi r \delta r}{\frac{\pi D_{tip}^2}{4}} \tag{18a}$$

$$C_{P,th}(\lambda)\left(\equiv \frac{P_{th}(\lambda)}{\frac{1}{2}\rho c_0^3 \frac{\pi D_{tip}^2}{4}}\right) = \frac{\sum\limits_{\text{all CA's}} C_{P,CA}(\lambda) 2\pi r \delta r}{\frac{\pi D_{tip}^2}{4}} \tag{18b}$$

A number of supplementary semi-empirical models are required to take into account effects that had been neglected so far. For instance, friction was partly excluded resulting in a theoretical $C_{P,th}$. or: At the blade tip a radial flow component develops causing a tip vortex. And the root region of the blade in the vicinity of the hub is affected by vortex type secondary flows.

A customary model for the flow in the blade root and tip region is due to BETZ/PRANDTL and Glauert [11] (see e.g., a summary in Sorensen [12], Gasch and Twele [6], Moriaty and Hansen [13]). The thrust and power coefficients derived from momentum conservation (Eq (15a,b)) are modified by a factor F_1 that gradually reduces the axial and tangential forces from those CA's which are located close to the blade tip and the hub:

$$C_{T,CA} = F_1 \cdot 4a(1-a) \tag{19a}$$

$$C_{P,sh,CA} = F_1 \cdot 4a'(1-a)\left(\frac{r}{r_{tip}}\lambda\right)^2 \tag{19b}$$

with

$$F_1 = \frac{4}{\pi^2}\arccos\left(\exp\left(\frac{B}{2}\frac{1-\frac{r}{r_{tip}}}{\frac{r}{r_{tip}}\sin\beta_\infty}\right)\right)\cdot\arccos\left(\exp\left(\frac{B}{2}\frac{\frac{r}{r_{tip}}-\frac{r_{hub}}{r_{tip}}}{\frac{r}{r_{tip}}\sin\beta_\infty}\right)\right) \tag{20}$$

Since the flow "leaks" around the blade tip from pressure to suction side, lift and drag of airfoil sections in the tip region are different from what the infinite span polar data suggest. Shen et al. proposed in [14] a correction

$$F_2 = \frac{2}{\pi}\arccos\left[\exp\left(-\left(\exp\left(-0.125\left(B\lambda-21\right)\right)+0.1\right)\frac{B}{2}\frac{1-\frac{r}{r_{tip}}}{\sin\beta_\infty}\right)\right] \tag{21}$$

that is incorporated into Eq (17a,b):

$$C_{T,CA} = \frac{B\ell}{2\pi r}\left(\left(1-a\right)^2+\left(\frac{r}{r_{tip}}\lambda\right)^2\left(1+a'\right)^2\right)\cdot F_2\cdot\left(C_L\cos\beta_\infty + C_D\sin\beta_\infty\right) \tag{22a}$$

$$C_{P,CA} = \frac{B\ell}{2\pi r}\left(\left(1-a\right)^2+\left(\frac{r}{r_{tip}}\lambda\right)^2\left(1+a'\right)^2\right)\cdot F_2\cdot\left(C_L\cos\beta_\infty - C_D\sin\beta_\infty\right)\frac{r}{r_{tip}}\lambda \tag{22b}$$

In practice, as the axial induction factor a exceeds a critical value $a_{crit} \approx 1/3$, complicated flow patterns result in much larger thrust coefficients as compared to the prediction by the basic BEM. Hence, Eq (14a) is replaced according to Buhl [15] by;

$$C_{T,CA} = \frac{8}{9}+\left(4F_1-\frac{40}{9}\right)a+\left(\frac{50}{9}-4F_1\right)a^2 \quad \text{for } a \geq 0.4. \tag{23}$$

As in the design part, the polar data of the infinite span airfoil sections are obtained via XFOIL. Post stall data, however, are obtained from Viterna et al. [16].

Some literature suggests solving the non-linear Eq (18a,b) with all their hidden supplementary model equations for a and a' explicitly (see e.g., the textbooks of Hansen [17] or Sørensen [12]). Since the authors encountered stability problems, an implicit scheme was set up [5]. It is encoded in our own inhouse MATLAB code, *deapWind,* which turned out to be very stable and reliable.

2.3. Converting non-dimensional into dimensional performance characteristics

Once the non-dimensional performance characteristics are known, it is trivial converting them into dimensional:

$$n = \lambda\cdot\frac{c_0}{\pi D_{tip}}, \quad P_S(n) = C_P(n)\cdot\frac{\rho}{2}\frac{\pi}{4}D_{tip}^2c_0^3 \; M_S(n) = C_M(n)\cdot\frac{\rho}{2}\frac{\pi}{8}D_{tip}^3c_0^2, F_{ax}(n) = C_T(n)\cdot\frac{\rho}{2}\frac{\pi}{4}D_{tip}^2c_0^2 \tag{24a, b, c, d}$$

It is worth noting that the value of Re stays the same only, if the size of the turbine D_{tip} is preserved and c_0 equals the design wind speed $c_{0,design}$. If the dimensional performance curves are required for other than the original design parameters, for instance for various wind speeds c_0, two options are possible: Either eqs. (24a,b,c,d) are used neglecting the effect of Re, or running the performance prediction scheme as described in section 2.2 for each c_0. The first option is faster and often sufficient for most practical purposes.

3. Results

3.1. Exemplary parametric studies

The results of two parametric studies targeting at small wind turbines illustrate the outcome of the design and performance prediction method. The first study shows the effect of the choice of λ_{design}, the second the impact of the number of blades B chosen for the rotor.

For a design wind speed $c_{0,design}$ = 6 m/s three rotors with each a diameter D_{tip} = 3.0 m and λ_{design} = 4.5, 7.5 and 10 are designed. NREL's S83x airfoils are chosen which were originally designed as "a family of quiet, thick, natural-laminar-flow airfoils for 1 to 3 m-diameter turbines" (SOMERS [18]). In particular, the root, middle and outer part of the blades are made from S835, S833 and S834 airfoils with a thickness/chord ratio of 21, 18 and 15%, respectively.

Computing airfoil lift and drag polars with XFOIL requires an assumption how the initially laminar boundary layer becomes turbulent in chord wise direction on the airfoil pressure and suction side. Particularly at low Re, which are typical for small wind turbines, the chord wise position of the laminar/turbulent transition depends on many details. This has a substantial effect on the predicted lift and drag. XFOIL offers the option "natural transition", where the position of laminar/turbulent transition is calculated using the e^N-method with a chosen threshold amplification ratio of N_{crit}. N_{crit} is a measure of the quality of the flow incident to the airfoil with, 15 for very clean inflow, 1 for very “dirty” (corresponding to a free stream turbulence level of 2%) with the consequence of transition very close to the airfoil leading edge; in a second option, positions x/l (= 0: leading edge, = 1: trailing edge) at the pressure and suction side are specified where transition is forced at the latest, Drela [10].

In these two parametric studies N_{crit} is set to 1 with natural transition accordingly. The XFOIL-computed polars for the three BE’s at hub, mid-span and blade tip are depicted in Figure 7. At each BE α_{design} is chosen close to the most favorable minimum drag/lift ratio, ε. Table 1 shows the results for three-bladed rotors. Increasing values of λ_{design} lead to slimmer blades. As expected C_P always reaches its peak close to λ_{design} but stays with approx. 0.42 the same. Note that the theoretical (BETZ) limit is 0.59. C_M is affected severely by the choice of λ_{design}: The lower λ_{design}, the larger C_M. The effect of λ_{design} on C_T is mainly at $\lambda > \lambda_{design}$. The dimensional characteristics in the lower row throw further light on the properties of the different designs: Increasing λ_{design} shifts the peak power to larger rotor speeds, resulting in lower shaft torques. Nevertheless, the peak powers are very similar.

Table 1. Variation of design tip speed ratio λ_{design}; upper row: rotor layout; middle: non-dimensional performance characteristics (the original design wind speed was $c_{0,design}$ = 6 m/s, the rotor diameter D_{tip} = 3.0 m); lower: the dimensional performance characteristics for the rotor diameter D_{tip} = 3.0 m at various wind speeds and air density, ρ = 1.2 kg/m^3 as from Eq (24a–d)

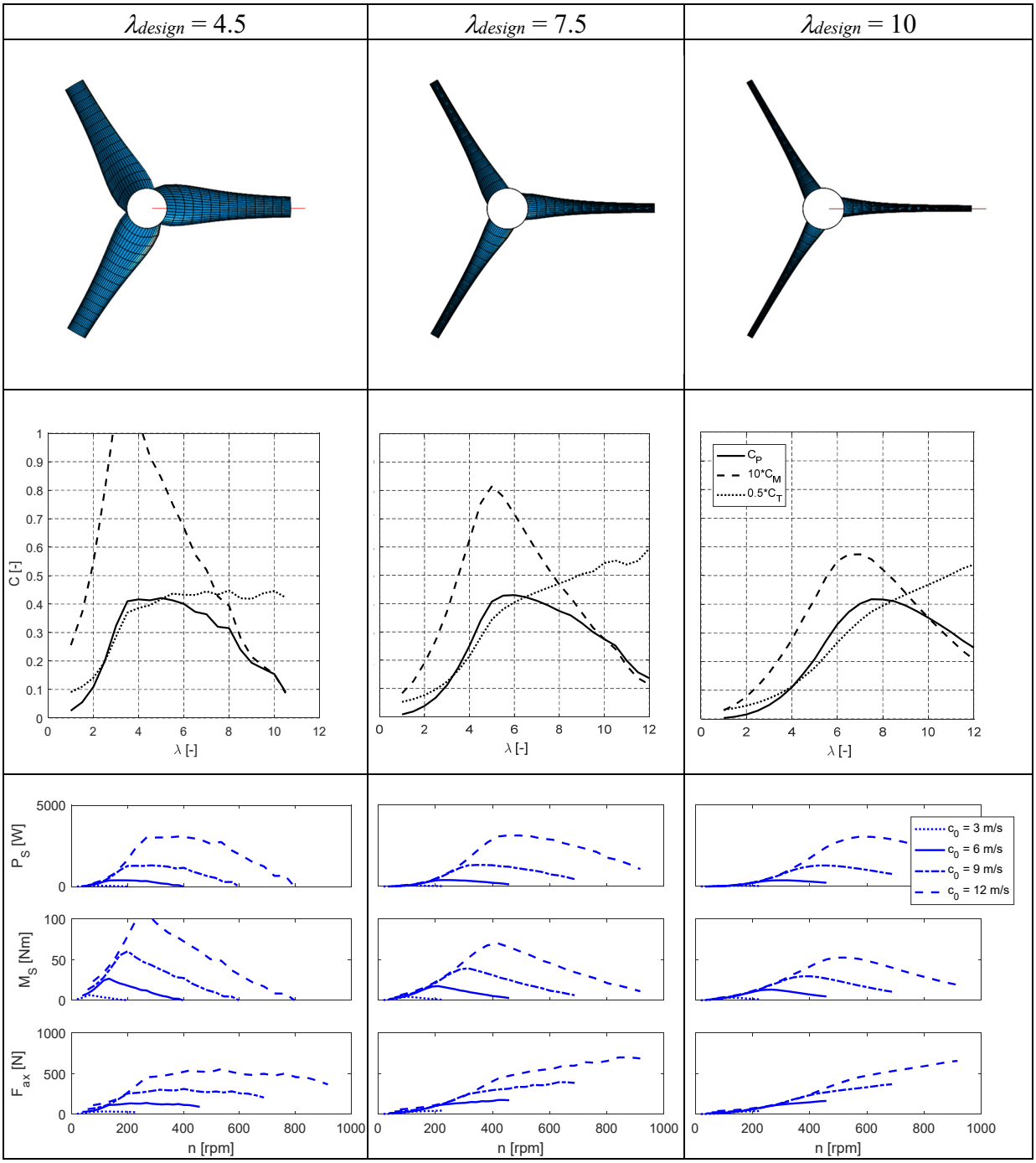

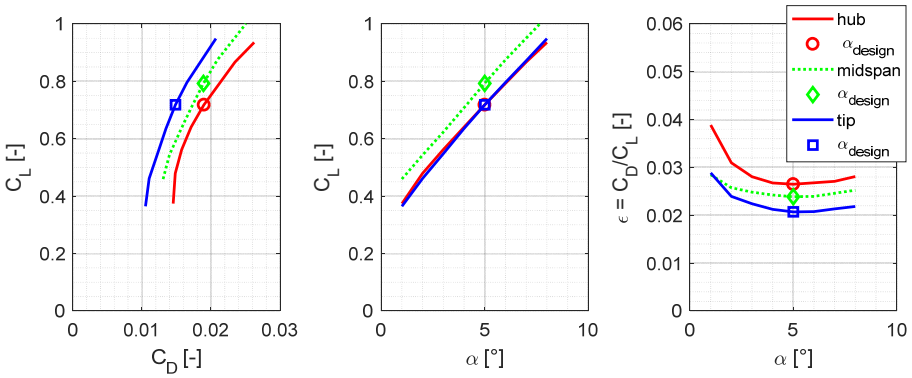

Figure 7. XFOIL-computed polars and design angles of attack α_{design} chosen (N_{crit} = 1, natural laminar/turbulent transition).

A frequent but naive argument is to increase the number of blades for more power. The results of a variation of number B of blades chosen while keeping λ_{design} = 7.5 are compiled in Table 2. The performance characteristics are very similar, irrespective of the number of blades chosen. It must be noted that the spanwise distribution of solidity and blade pitch of all three rotors is kept the same as obtained by Eqs (9,10). The minor effect of B stems from the impact of Re and those loss mechanisms that are a function of B. Hence, a criterion for the choice of B—among others—is the technical practicability of many slim or a few more massive blades, but not the power output.

3.2. Case study: Micro wind turbine with battery charger

The objective of this exemplary case study is the design of a HAWT for a small generator/battery charger. The analysis involves matching the wind turbine rotor performance curves to the torque characteristic of the battery charger. Upon manufacturing, a concluding wind tunnel experiment validates the theoretical analysis.

3.2.1. Available wind resource and turbine specification

Starting point is a one-year histogram of measured wind speed data collected at the candidate site, which is the campus of Dedan Kimathi University of Technology, Nyeri in central Kenya. The wind data were monitored from December 2016 to December 2017. The data includes the measured wind speeds and directions. Figure 8 visualizes the hours of occurrence of the ten (10) minutes averages of prevailing wind speeds at this site. Obviously, at this site wind speeds in the 4, 5 and 6 m/s wind speed bins are most prevalent. For the micro turbine to be designed $c_{0,design}$ = 6 m/s is chosen. The specified air density is ρ = 1.058 kg/m^3, which corresponds to the altitude above sea level of the planned site for the turbine.

Table 2. Variation of number B of blades chosen (λ_{design} = 7.5, $c_{0,design}$ = 6 m/s, D_{tip} = 3.0 m).

B = 2	B = 3	B = 5
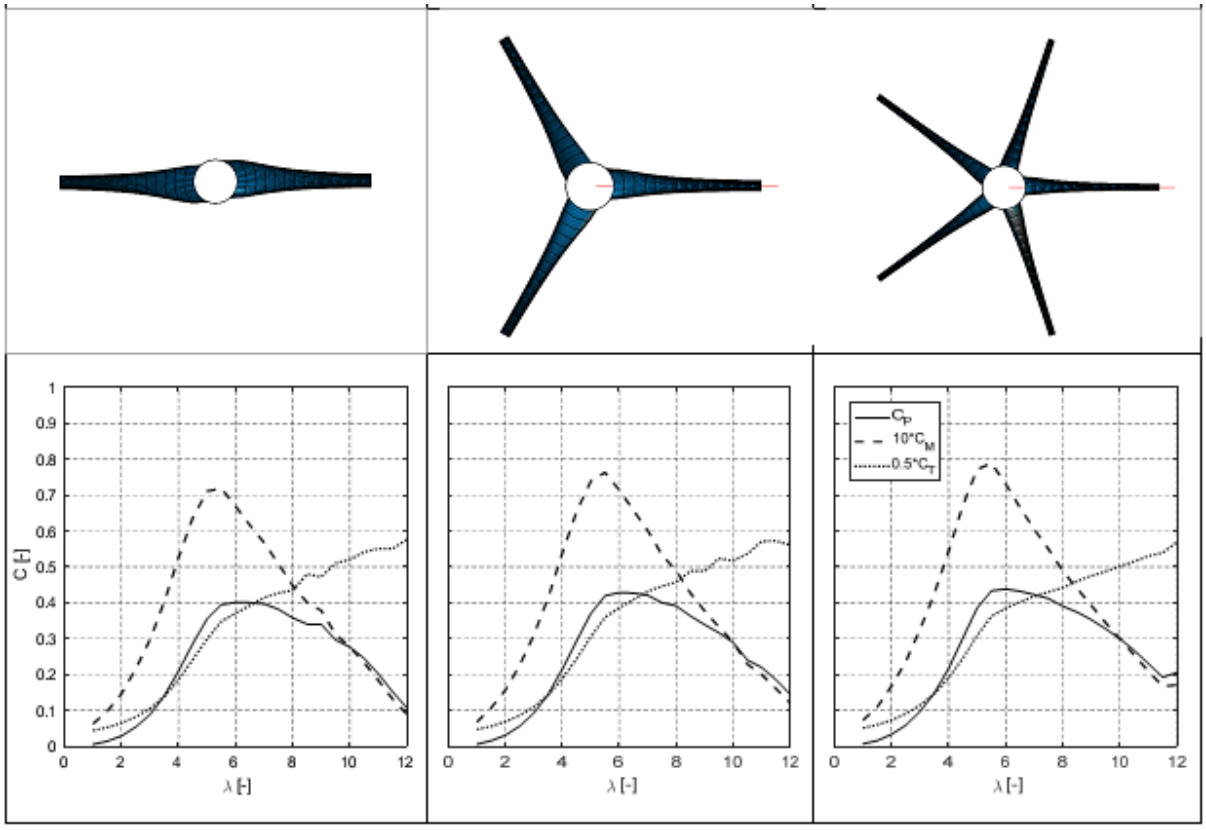		

At any rotor speed *n,* the shaft torque provided by the turbine rotor must equal the torque required by the electric generator:

$$M_{S,Turb}=M_{S,Gen} \tag{25}$$

The generator/charger unit characteristic $M_{S,Gen}(n)$, is determined experimentally by coupling the shaft of the electric generator to an auxiliary electric motor. The torque required by the generator is measured for any set speed via a torque measurement shaft in-between. The measured generator/charger characteristic for the controller status "Battery empty—charge" is the red curve in the middle graph of Figure 10.

It is worth to note that for maximum energy yield the generator/charger characteristic should be a quadratic parabola. Once parameterized correctly this would enable to operate the turbine at maximum C_P for any c_0. This strategy is provided by more advanced controllers or grid-connected turbines. In contrast, objective of this case study is the aerodynamic design of a rotor to the given generator/charger characteristic that ensures unambiguous rotor speed for any wind speed, keeps the rotor diameter as small as possible and provides a maximum annual energy output for the given wind resource.

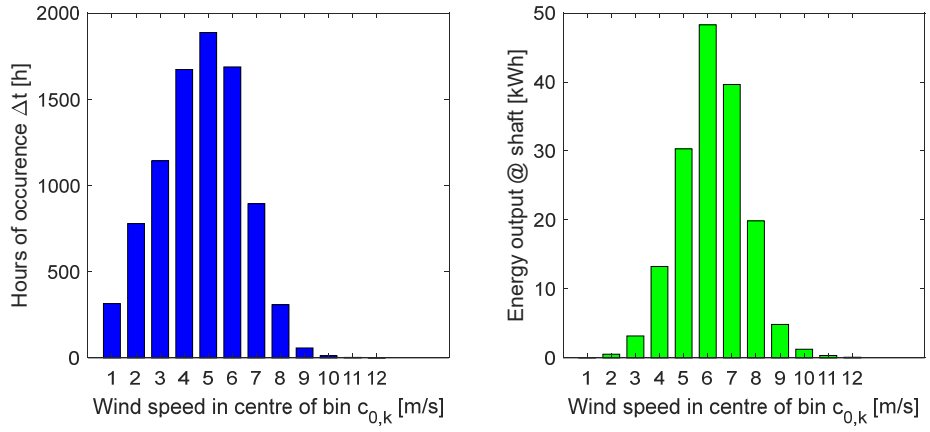

Figure 8. Left: Hours of occurrence of the 10 minute averages of prevailing wind speeds (histogram) at Dedan Kimathi University of Technology, Nyeri, in central Kenya $c_{0,k}$ is the centre of a wind speed bin with a band width Δc_0 = 1 m/s; right: Predicted electric energy output with the rotor/generator assembly as in section 3.2.3 for an air density ρ = 1.058 kg/m^3.

3.2.2. Electric generator/battery charger

The electric generator/battery charger unit consists of three main components:

- The electric generator; the turbine rotor is attached to the shaft of the generator without gearbox
- The battery to be charged
- The control unit, essentially comprising a 3-phase rectifier, a charge controller, a voltage threshold switch acting on a power relay which connects the generator to a load resistor rather to the charge controller, and a supply point to consume e.g., USB ports for charging wireless phones.

Its layout is depicted in Figure 9. The charge controller distinguishes between the bulk mode "Battery empty—charge with a current up to 2 A" and the float mode "Battery full—trickle charge with 0.6 A". Power provided by the turbine rotor but not absorbed by the battery is dumped via the load resistor. Voltage and current at the charge controller can be monitored via Bluetooth® on a smart phone.

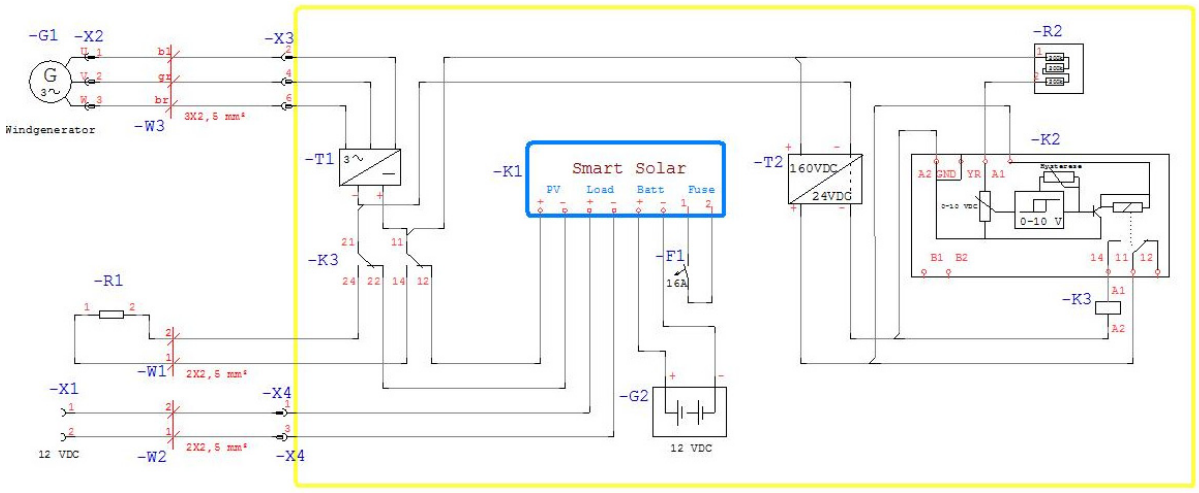

Figure 9. Components and layout of the generator/battery charger circuit; G1: Electric generator ElvWiS™ ADVENTURE GEA-200-AL (100/225W), G2: Sealed lead acid battery WP12-12E (12 V, 12Ah), K1: Charge Controller (Smart Charge MPPT 100/15, victronenergy™), K2: Threshold switch acting on power relay K3, R1: Load resistor, X1: Supply point to consumer, e.g., USB ports for charging wireless phones.

3.2.3. Turbine rotor selection

Different turbine rotor types with λ_{design} ranging from 3.0 to 5.0 and D_{tip} from 0.8 m to 1.3 m have been designed. The hub diameter is fixed to 0.19 m in order to fit to the outer diameter of the electric generator. Mainly for low manufacturing cost, the rotor is two-bladed. Laminar/turbulent transition was fixed to $x/l = 0.02$ on each BE suction side and 0.05 on the pressure side, assuming that the foreseen method of manufacture does not yield to perfect smooth and precise blade surfaces, with the consequence of laminar/turbulent transition close to the blade leading edge.

Relevant parameters of some of the rotor/charger assemblies are compiled in Table 3. One criterion for selection is the annual energy output at the shaft of the rotor

$$AEO_S = \sum_{\text{all } k \text{ bins}} C_{P,k} \frac{\rho}{2} \frac{\pi}{4} D_{tip}^2 c_{0,k}^3 \cdot \Delta t_k \tag{26}$$

which translates into the electric energy output when subtracting all electric losses. Other criterions are the rotor speed at the most prevalent wind speed 6 m/s and at high winds, here 12 m/s. Low rotor speeds are easier to handle and produce less noise. Also, the axial thrust is a criterion. Large axial thrust forces require more expensive structures to hold the turbine.

Table 3. Variants of rotor/charger assemblies and selected performance parameters for ρ = 1.058 kg/m^3.

	D_{tip} [m]	λ	AEOs [kWh/a]	n at c_0 = 6 m/s [rpm]	n at c_0 = 12 m/s [rpm]	F_{ax} at c_0 = 12 m/s [N]	Remarks
1	0.8	4.0	108	500	1990	28	lowest AEOs, glancing intersection of torque curves at high c_0 may yield ambiguous rotational speeds
2	1.0	3.0	132	530	1250	31	low AEOs
3	1.0	4.0	162	560	1690	44	best compromise
4	1.0	5.0	176	580	1990	51	Largest n @ c_0 = 12 m/s largest D_{tip}
5	1.2	4.0	181	591	1470	64	large D_{tip}, large T @ c_0 = 12 m/s [N]
6	1.3	4.0	168	591	1360	73	large D_{tip}, largest T @ c_0 = 12 m/s [N]

The rotor ultimately selected has the parameters D_{tip} = 1 m and λ_{design} = 4.0. Important geometrical parameters of each BE are compiled in Table 4. Figure 10 illustrates the synthesis of the measured generator characteristic ("mode Battery empty—charge", red line with red crosses in the middle diagram) and this rotor at different wind speeds; the black circles indicate the operating points of the complete assembly. Figure 8 right shows the predicted shaft energy output at each wind speed bin of the turbine/generator assembly.

Table 4. Geometrical parameters of the blade forthe rotor: D_{tip} = 1 m, λ_{design} = 4.0, $c_{0,\text{design}}$ = 6 m/s.

BE	r/r_{tip}	L [m]	γ [°]
1	0.190	0.306	29.178
2	0.248	0.300	24.236
3	0.306	0.284	20.326
4	0.364	0.265	17.223
5	0.421	0.246	14.738
6	0.479	0.229	12.721
7	0.537	0.214	11.069
8	0.595	0.201	9.693
9	0.653	0.189	8.540
10	0.711	0.179	7.562
11	0.769	0.170	6.726
12	0.826	0.162	6.006
13	0.884	0.155	5.382
14	0.942	0.149	4.835
15	1.000	0.143	4.358

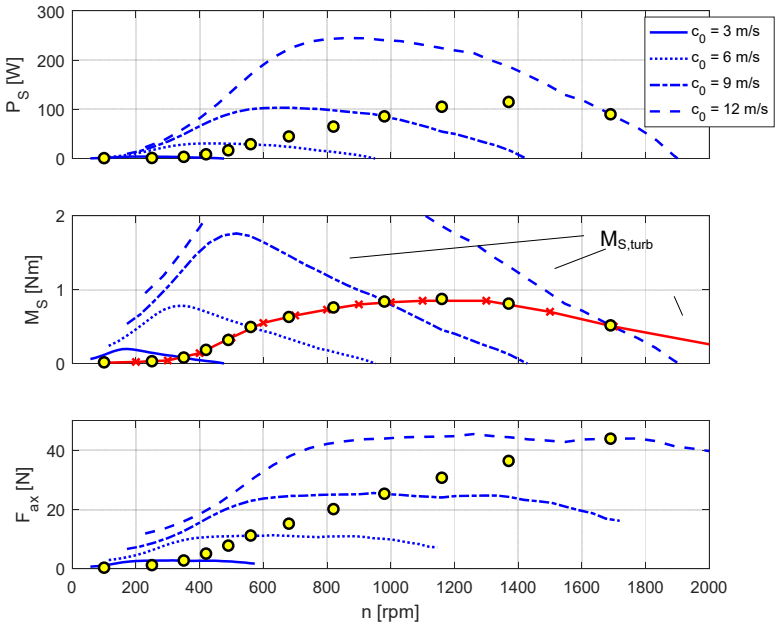

Figure 10. Synthesis of measured generator torque characteristic (bulk mode "Battery empty—charge", red line with red crosses in the middle diagram) and turbine characteristics (blue) at different wind speeds and an air density ρ = 1.058 kg/m^3; the circles indicate the predicted operating points of the complete assembly at c_0 = 1, 2, … 12 m/s

3.2.4. Manufacture of turbine rotor

The software *deapWind* yields the BE coordinates of 15 BE's along the span. From that a 3D CAD model and 2D technical drawings are established. For manufacturing a traditional technique is chosen that requires a standard carpenter's workshop only: The blades are carved from a high quality wood block with the help of a grid of drill holes, Figure 11. The perpendicular distance from each of the grid point on the blade surface to the surface of the block is measured in the 3D CAD model. This is performed for both sides of the blade. This distance is the depth of the 8 mm holes to be drilled. The drilling of the holes is to ensure that the correct depth of material removal is achieved. It acts as a guide on the maximum depth of material removal obtain the blade profile. The material was removed manually to almost the end of the drilled holes that mark the surface of the blades. The finishing was done using rough and fine sand papers. In order to achieve the finest surface finish, the blades were applied with wood filler, allowed to dry up, then filed using the finest sand papers. At the hub, the material removal and smoothening was achieved by use of rough and fine wood files.

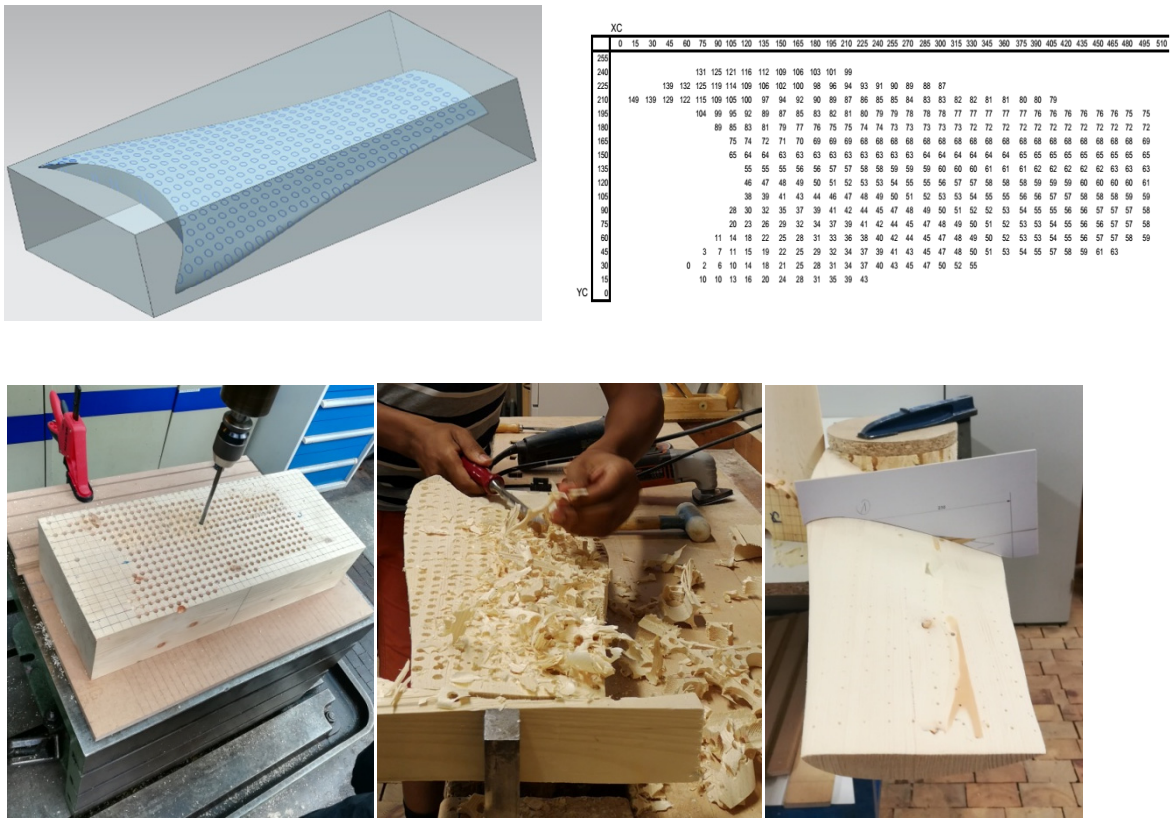

Figure 11. Fabrication of the blades; upper: 3D CAD model and drilling plan; lower: wood block to blade process.

3.2.5. Wind tunnel validation test

For the experiments, the rotor was mounted upstream on the drive train, comprising a steel shaft, separate bearings and the electric generator. The battery charger was connected to the generator. The complete assembly was tested in the University of Siegen wind tunnel. This wind tunnel is a closed-circuit type allowing a maximum wind speed of the wind tunnel of 70 m/s at a turbulence intensity less than 0.35%. Figure 12 shows the experimental set up in the wind tunnel (all dimensions are in millimeters). The wind speed was measured using a propeller anemometer, the rotational speed with an optical laser tachometer. The wind speed was varied in steps. Upon steady-state operation, the rotational speed of the turbine was recorded. It is important to note that the air density in the wind tunnel lab was approx. ρ = 1.17 kg/m^3, resulting in different dimensional turbine performance characteristics as compared to those in the previous sections. This has been taken into account. Ideally, the shaft power of the rotor would have been measured. This was not possible. The electric power was measured instead.

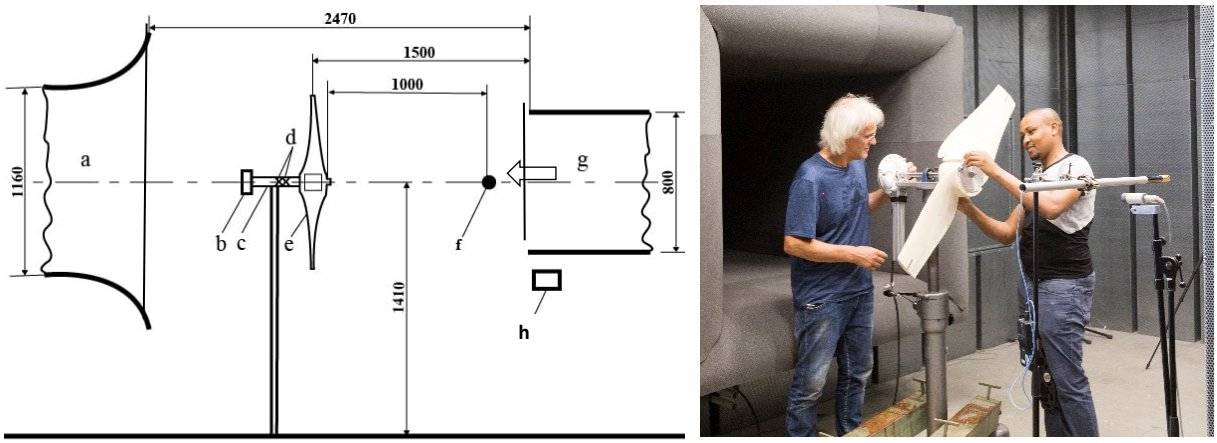

Figure 12. Experimental setup in the University of Siegen wind tunnel (all dimensions in mm); a—wind tunnel collector, b—electric generator, c—shaft, d—bearings, e—wind turbine rotor, f—propeller anemometer, g—wind tunnel nozzle, h—optical laser tachometer (rotor speed).

A comparison of the rotational speed of the complete rotor/charger assembly in bulk mode ("Battery empty—charge") at different wind speeds is depicted in Figure 13 left. Obviously, the "loading" of the rotor by the electric generator is very close to what was expected from the previous analysis. This partly validates the aerodynamic rotor design. The difference of predicted rotor shaft power and the measured electric power, Figure 13 right, is an indicator for the electric overall efficiency

$$\eta_{el} \equiv P_{el}/P_S \tag{27}$$

of the complete assembly. A major loss is attributed to the electric generator. Its electric efficiency characteristic was measured separately—similarly as the complete generator/charger/battery characteristics before, and is depicted for n = 560 rpm in Figure 14. At P_S = 29 W (corresponding to c_0 = 6 m/s) the generator's electric efficiency is 47%. Other electric losses stem from the battery charger, and—up from c_0 = 7.5 m/s—then active load resistor for protecting the battery. Eventually, fundamental errors due to blockage of the wind tunnel test section by the rotor and a potentially reduced turbine efficiency due to the manual manufacture may account for a lower than predicted power coefficient of the rotor. Note, that the turbine shaft power could not be measured directly during the wind tunnel measurement campaign.

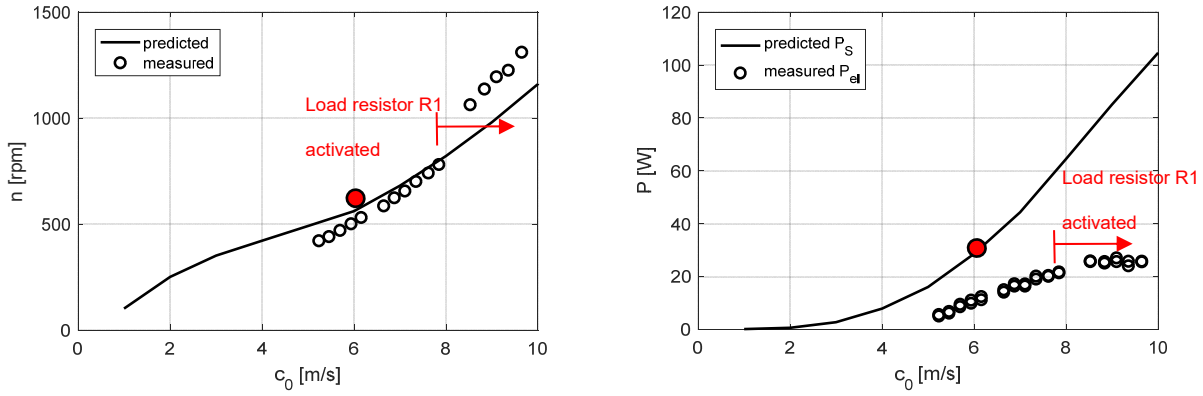

Figure 13. Wind tunnel test of the complete rotor/charger assembly in bulk mode ("Battery empty—charge") at different wind speeds, air density ρ = 1.17 kg/m^3, left: Rotational speed vs. wind speed, right: Predicted shaft and measured electric power; the red filled circles denote the predicted operating point at c_0 = 6 m/s

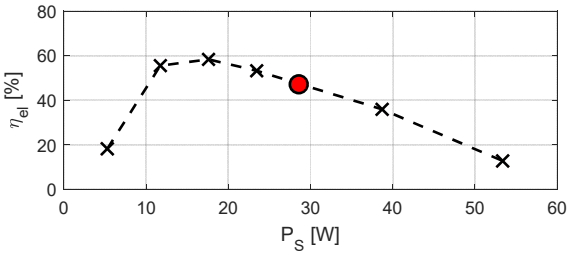

Figure 14. Experimentally determined electric efficiency of the isolated electric generator and generator operating point (red circle) when integrated into the rotor/charger/battery assembly and operating at n = 560 rpm, corresponding to c_0 = 6 m/s.

4. Summary and conclusions

An analytical method for the aerodynamic design of horizontal of axis wind turbines including performance prediction was described. The underlying theory for design and shaft power and thrust force prediction is an advanced version of the well-established blade-element-momentum (BEM) theory, encoded in our own in-house MATLAB™ code *deapWind*. The procedure yields the geometry of the aerodynamically profiled and twisted blades which are designed to yield maximum power output for a given design wind speed.

Two parametric studies illustrated typical outcomes of the design and performance prediction method: (i) A variation of the design tip speed ratio λ_{design}; the higher λ_{design} the larger the rotational speed at a given wind speed and the smaller the torque. Hence, the choice of λ_{design} allows to match the turbine to sites with either low or high mean wind speeds. Moreover, the higher λ_{design} the slimmer the blades, which may have an impact on manufacture and structural health. (ii) A variation of the number of blades B in a rotor, while keeping λ_{design} constant; as expected the results proved that the non-dimensional turbine performance characteristics are nearly independent of the number of blades chosen; a minor effect of B stems from the impact of Re and the various aerodynamic loss mechanisms

taken into account in the advanced blade-element-momentum theory. Hence, a criterion for the choice of *B*—among others—is the technical practicability of many slim or a few more massive blades, but not the power output as occasionally naively proposed.

Eventually, a more comprehensive case study dealt with a micro wind turbine for a small low cost generator/battery charger. A goal was to foresee turbine blades of high aerodynamic quality that can be manufactured with techniques available in less developed regions of the world. The analysis involved matching the turbine rotor performance curves to the torque characteristic of the battery charger, manufacture of the rotor and a concluding wind tunnel experiment for validation of the theoretical analysis. Starting point was a one-year histogram of measured wind speed data collected at the candidate site in rural central Kenya. Prior to the wind turbine design, the generator torque/speed characteristic was determined experimentally in a laboratory by coupling the shaft of the electric generator to an auxiliary electric motor. The torque was measured for any set speed via a torque measurement shaft in-between. The generator was connected to the charge controller and empty battery. The interplay of various turbine rotors and the drive train/battery charging was simulated. Criterions for selection of the rotor were the annual energy output at the shaft, the rotor speed at the most prevalent wind speed and at high winds, and the axial thrust exerted on the rotor by the wind. A blade manufacturing technique was chosen that requires a standard carpenter's workshop only. Compared to 3D printing and additive manufacturing, this technology is simple, cheap and accessible to less developed nations for developing wind turbines for providing energies to communities off the national grids. Finally, the complete rotor/drive train//battery charger assembly was tested in the University of Siegen wind tunnel. The rotational speed for various wind speeds are very close to what was expected from the previous analysis. This partly validates the aerodynamic rotor design. The difference of predicted rotor shaft power and measured electric generator power. i.e., the value of the overall electric efficiency, is mainly attributed to the electric losses in the generator and the battery charger circuit.

Upcoming efforts must provide for passive yaw and storm protection. A tail vane can act as a passive yaw system, or a downwind installation of the rotor. The predicted thrust may facilitate the design of any mechanical tilt mechanism and eventually dimensioning of the tower. Safe cut-out at high winds and early cut-in of the turbine can be assisted by an advanced electric control.

Author contributions

S. K. Musau designed and manufactured the micro turbine described in the case study. K. Stahl assisted in designing the turbine including the electric part and guided the wind tunnel experiments and data evaluation. K. Volkmer created the software *deapWind* by linking an extended version of an existing wind turbine design method with N. Kaufmann's turbine performance prediction procedure. Th. Carolus is the leader for the project and compiled the manuscript with the help of all co-authors.

Acknowledgment

The project was partly funded by the Erasmus+ Programme of the European Union (Key Action 107 Mobility with partner countries). Partner were the University of Siegen and Dedan Kimathi University of Technology, Kenya. The authors gratefully appreciate this financial support. The authors also want to thank S. Kreklow and T. Schönemann from the University of Siegen electronic workshop for the design of the electronic circuits, J. Janssens from the mechanical workshop for the assistance in

manufacturingthe turbine blades, A. Bald for providing the test opportunity of the wind turbine in the University Siegen aeroacoustic wind tunnel and B. Homrighausen supervising the complete project. Special thanks also Harrison T. Ngetha for his support.

Conflict of interest

To the best of our knowledge, there is no conflict of interest.

References

1. European Commission, FP 7. Available from: https://cordis. europa.eu (assessed April 08, 2020).
2. RenewableUK, Small Wind Turbine Standard (15 January, 2014). Available from: https://mcscertified.com/wp-content/uploads/2019/08/RenewableUK-Small-Wind-Turbine-Standard-2014-01-05.pdf (assessed April 04, 2020).
3. Jütemann P, Kleinwind-Marktreport 2020. Available from: http://www.Klein-Windkraftanlagen.com ((assessed April 04, 2020).
4. ARGE Lichtenegg, Wien, Austria. Available from: http://www.energieforschungspark.at (assessed April 04, 2020).
5. Kaufmann N, "Small Horizontal Axis Free-Flow Turbines for Tidal Currents," ISBN 978-3-8440-6705-7. Shaker-Verlag Düren, 2019.
6. Gasch R, Twele J (2013) Windkraftanlagen: Grundlagen, Entwurf, Planung und Betrieb. 8th ed. Stuttgart: Springer Vieweg.
7. Gerhard T, Sturm M, Carolus T (2013) Small Horizontal Axis Wind Turbine: Analytical Blade Design and Comparison with RANS-Prediction and Experimental Data. *Proceedings of the ASME Turbo Expo* 2013.
8. Betz A (1994) Windenergie und ihre Ausnutzung durch Windmühlen: 1926. Reprint Ökobuch Freiburg, 1994.
9. Drela M (2013) XFOIL—Subsonic Airfoil Development System, 2013.
10. Drela M (2003) Implicit Implementation of the Full e^n Transition Criterion. *In 21st AIAA Applied Aerodynamics Conference, Orlando, Florida*, 2003.
11. Glauert H (1935) Airplane Propellers, in Aerodynamic Theory: A General Review of Progress Under a Grant of the Guggenheim Fund for the Promotion of Aeronautics. W. F. Durand, Ed., Berlin, Heidelberg: Springer Berlin Heidelberg, 169–360.
12. Sørensen JN (2016) General Momentum Theory for Horizontal Axis Wind Turbines. 1st ed. s.l.: Springer-Verlag, 2016.
13. Moriarty PJ, Hansen AC (2005) AeroDyn Theory Manual. Golden, CO: National Renewable Energy Laboratory, 2005.
14. Shen WZ, Mikkelsen R, Sørensen JN, et al. (2005) Tip loss corrections for wind turbine computations. *Wind Energy* 8: 457–475.
15. Buhl ML (2005) New Empirical Relationship between Thrust Coefficient and Induction Factor for the Turbulent Windmill State. *Technical Report: NREL/TP-500-36834, National Renewable Energy Laboratory, Golden, CO*, 2005.
16. Viterna LA, Corrigan RD (2008) Fixed pitch rotor performance of large horizontal axis wind turbines. *In DOE/NASA Workshop on Large Horizontal Axis Wind Turbines*, Cleveland, 1981.

17. MOL Hansen (2008) Aerodynamics of Wind Turbines. London: Earthscan, 2008.
18. DM Somers (2005), The S833, S834, and S835 Airfoils, National Renewable Energy Laboratory Report No. NREL/SR-500-36340, Golden, Colorado, USA 2005.
19. Chen Y, Mendoza ASE, Griffith DT, et al. (2021) Experimental and numerical study of high-order complex curvature mode shape and mode coupling on a three-bladed wind turbine assembly. *Mech Syst Signal Process* 160: 107873.
20. Chen Y, Joffre, Avitabile P (2018) Underwater dynamic response at limited points expanded to full —field strain response. *J Vib Acoust*, 2018.
21. Chen W, Jin M, Huang J, et al. (2021) A method to distinguish harmonic frequencies and remove the harmonic effect in operational modal analysis of rotating structures. *Mech Syst Signal Process* 161: 107928.
22. Ceyhan O (2008) Aerodynamic design and optimization axis wind turbines by using BEM theory and genetic Algorithm.
23. Clifton-Smith MJ, Wood DH (2007) Further Dual purpose evolutionary optimization of small wind turbine blades. *J Phys Conf Ser*.
24. Liu X, Chen Y, Ye Z (2007) Optimization model for rotor blades of horizontal axis wind turbines. *Front Mech Eng* 2: 483–488.
25. Lee MH, Shiah YC, Bai CJ (2016) Experiments and numerical simulations of the rotor blade performance for a small-scale horizontal axis wind turbine. *J Wind Eng Ind Aerodyn* 149: 17–29.
26. Lanazafame R, Messina M (2007) Fluid dynamics wind turbine design: Critical analysis, optimization and application of BEM theory. *Renewable Energy* 32: 2291–2305.

AIMS Press